A Combined ^{25}Mg Solid-State NMR and *ab initio* DFT Approach to Probe the Local Structural Differences in Magnesium Acetate Phases $Mg(CH_3COO)_2{\cdot}nH_2O$ (n = 0, 1, 4)

Dr. Valerie R. Seymour[a], Dr. Stephen P. Day[b], Dr. Gudrun Scholz[c], Dr. Kerstin Scheurell[c], Dr. Dinu Iuga[b], Dr. John M. Griffin[a,d], Prof. Dr. Erhard Kemnitz[c], Dr. John V. Hanna[b] and Prof. Mark E. Smith[a,e]*

[a] Dr. V. R. Seymour, Dr. J. M. Griffin, and Prof. M. E. Smith
Department of Chemistry, Lancaster University,
Bailrigg, Lancaster, LA1 4YB, UK
Email: m.e.smith@lancaster.ac.uk

[b] Dr. S. P. Day, Dr. D. Iuga, and Dr. J. V. Hanna
Department of Physics, University of Warwick,
Coventry, CV4 7AL, UK

[c] Dr. G. Scholz, Dr. K. Scheurell, and Prof. Dr. E. Kemnitz
Department of Chemistry, Humboldt-Universität zu Berlin,
Brook-Taylor Str. 2, D-12489 Berlin, Germany

[d] Dr. J. M. Griffin
Materials Science Institute, Lancaster University,
Bailrigg, Lancaster, LA1 4YB, UK

[e] Prof. M. E. Smith
Vice-Chancellor's Office,
University House, Lancaster University, Bailrigg, Lancaster, LA1 4YW, UK.

Corresponding author: Mark E. Smith
Department of Chemistry, Lancaster University, Bailrigg, Lancaster, LA1 4YB, UK
Email: m.e.smith@lancaster.ac.uk

Abstract

Multinuclear (^{1}H, ^{13}C, ^{25}Mg) solid-state NMR data is reported for a series of magnesium acetate phases $Mg(CH_3COO)_2{\cdot}nH_2O$ (n = 0 (two polymorphs), 1, 4). The central focus here is ^{25}Mg as this set of compounds provides an expanded range of local magnesium coordinations compared to what has previously been reported in the literature using NMR. These four compounds provide 10 distinct magnesium sites with varying NMR interaction parameters. One of the anhydrous crystal structures (α) has an MgO_7 site which is reported, to the best of our knowledge, for the first time. For those phases with a single crystal structure, a combination of magic angle spinning (MAS) NMR at high magnetic field (20 T) and first principles density functional theory (DFT) calculations demonstrates the value of including ^{25}Mg in NMR crystallography approaches. For the second anhydrate phase (β), where no single crystal structure exists, the multinuclear NMR data clearly show the multiplicity of sites for the different elements, with ^{25}Mg satellite transition (ST) MAS NMR revealing four inequivalent magnesium environments, which is new information constraining future refinement of the structure. This study highlights the sensitivity of ^{25}Mg NMR to the local environment, an observation important for several sub-disciplines of chemistry where the structural chemistry of magnesium is likely to be crucial.

Introduction

The isotope-specific nature of NMR spectroscopy can provide information on the local, atomic-scale structure of a compound from each NMR-active element's perspective. Traditionally by determining the NMR parameters (*e.g.*, chemical shift, quadrupolar, *etc*.) from spectra for a nucleus in well-known local environments, unknown environments can be identified by a simple comparison of the NMR spectra and parameters extracted. The utility of NMR to a wide range of inorganic materials is well understood,[1] although not all nuclei are equally amenable, so that NMR studies tend to be dominated by those nuclei with larger magnetic moments and hence higher Larmor frequencies. In more recent times as the experimental capability of NMR has greatly improved,[2] especially through the availability of ultra-high magnetic fields, a greater number of nuclei have become more readily accessible. Also the ability to calculate NMR parameters using first principles calculations has greatly improved in recent years.[3,4] The comparison of experimentally determined NMR parameters, with calculations of those parameters combined with iterative refinements of the structure has led to what has become termed NMR crystallography.[5]

Nuclei with smaller magnetic moments (termed low-γ nuclei) have become much more amenable in recent years, with the advent of ultra-high magnetic fields. [1] The utility of ultra-high fields for low-γ nuclei is especially true for those with nuclear spin I > ½, since under magic angle spinning (MAS), the residual second-order quadrupolar broadening effects which typically dominate spectra, scale inversely with the applied magnetic field (*i.e.* are reduced with increasing applied magnetic field).[1,6] Magnesium-25 is amongst this group of nuclei. Magnesium is an important element in technological ceramics and glasses, earth science, molecular organic frameworks (MOFs) and biomolecular systems. However knowledge of local coordination environments of Mg^{2+} cations is still limited, but in principle could be supplied by ^{25}Mg solid-state NMR experiments. As well as being low-γ quadrupolar nucleus, observation of ^{25}Mg is also hampered by its low natural abundance (10.1%). These complications (low-γ, low natural abundance) meant that the very early ^{25}Mg MAS NMR studies were limited to compounds where the magnesium was in more highly symmetric local environments.[7]

With increased routine access to higher magnetic fields (≥ 18.8 T) a more representative range of magnesium environments in organic and inorganic magnesium oxo-compounds using natural abundance ^{25}Mg solid-state NMR measurements has started to appear.[8,9] Both these studies[8,9]

combined experimental and computational approaches, showing that the NMR parameters (usually both the chemical shift and quadrupolar) could be extracted and were sensitive to the local environment around magnesium. Applications where ^{25}Mg solid-state NMR has provided insight into the structural chemistry of magnesium include the earth sciences. For enstatite ($MgSiO_3$), all three polymorphic forms contain two crystallographically-distinct magnesium sites, but MAS NMR spectra at both 14.1 and 20.0 T only showed a single site. Calculations indicated that the second site although still an MgO_6 had a much larger quadrupolar interaction (~5 times greater) and needed a variable offset cumulative spectroscopy (VOCS) approach to detect it as a much broader underlying second resonance.[10] For a different magnesium silicate, β-Mg_2SiO_4, comparing anhydrous and hydrous forms, the ordering of magnesium over the possible sites creates some ordered vacancy structures in the hydrous forms. Simulations showed that the ^{25}Mg NMR parameters are able to distinguish between the different vacancy arrangements on the magnesium sites.[11]

Extending ^{25}Mg NMR to more disordered systems, the spectra clearly show changes in site distribution of magnesium coordinations (*i.e.*, from predominantly MgO_6/MgO_5 to MgO_4) with composition in silicate glasses.[12] Changes of magnesium coordination in nanoscopic magnesium hydroxide fluorides produced by different chemical routes could be readily followed by ^{25}Mg NMR.[13] ^{25}Mg solid-state NMR has proved effective in studying magnesium-containing MOFs. Examples include the effect of guest species on the magnesium environment in CPO-27[14], probing the paraelectric-ferroelectric transition in $[NH_4][Mg(HCOO)_3]$[15] and demonstrating the unambiguous formation of five-coordinate magnesium centres in activated Mg_2(dobpdc).[16] Summaries of ^{25}Mg solid-state NMR data in the literature have been presented in two reviews.[17,18] Hence there looks to be significant promise in developing ^{25}Mg solid-state NMR as a probe of local structure, such that extending the combination of experimental and computational data from well-defined local magnesium environments will further increase the confidence and utility of this approach.

In 2012, some of the authors succeeded in synthesising new magnesium acetate solvates $Mg(OAc)_2$.nL, with L including different organic solvents and water (L: MeOH, EtOH, HOAc, H_2O), and their structures were determined using single crystal X-ray crystallography.[19] This present work reports on the hydrate system starting from water as solvent is studied, where $Mg(OAc)_2.4H_2O$ is available to buy commercially, and the $Mg(OAc)_2.H_2O$ can then be obtained by partial dehydration.

Water-free α-$Mg(OAc)_2$, can be obtained by complete dehydration, however using this approach in this study pure crystalline samples could not be obtained. An alternative approach using MgO as a starting material with acetic acid in ethyl acetate was employed here to synthesise some of the phases. This magnesium acetate system provides a range of crystal structures with different, crystallographically distinguishable lattice positions of Mg^{2+} cations, with some interesting local magnesium coordinations.

In the current study, multinuclear (^1H, ^{13}C, ^{25}Mg) solid-state NMR is reported for $Mg(OAc)_2.4H_2O$, $Mg(OAc)_2.H_2O$ and $Mg(OAc)_2$ with an emphasis on ^{25}Mg. The crystal structures based on single crystal work has been reported for these phases.[19] In Fig. 1 the local coordination around each magnesium site is shown from structures where there has been a single crystal determination. The combination of solid-state NMR measurements and first principles density functional theory (DFT) calculations provide valuable information regarding local structural details of the magnesium sites present. The tetrahydrate phase is readily available and several reports of the ^{25}Mg NMR parameters appear in the literature, of a single MgO_6 site with a relative modest quadrupolar constant (C_Q ~2.5 MHz), with the most recent higher field studies providing the most accurate values and were in good agreement.[8,9] No previous ^{25}Mg NMR data has been presented for the other phases, which offer two different six-fold coordinated Mg-sites in $Mg(OAc)_2.H_2O$, and three different Mg-sites in $Mg(OAc)_2$. For the latter compound the challenge of evaluating the NMR parameters of the superimposed signals from two MgO_6 and one MgO_7 coordination [Fig. 1] is possible by comparing a high-quality distortion-free one-dimensional MAS spectrum at 20.0 T with the DFT calculated parameters. It is believed that this is the first time the parameters from an MgO_7 coordination have been reported. In the course of preparing these phases a second anhydrate phase was formed, which agrees with a powder pattern in the literature.[20,21] No single crystal structure has been reported for this second anhydrate phase, but the NMR data can help determine the number of different sites present. In particular, to better constrain the ^{25}Mg NMR spectra a ^{25}Mg-enriched sample was made so that a two-dimensional (2D) satellite transition (ST) MAS spectrum could also be obtained. This ST-MAS approach[22] was chosen as it has better sensitivity than other comparable multiple quantum experiments as it only involves correlating single quantum transitions, and it reveals four distinct magnesium sites.

Results and Discussion

Preliminary Characterisation: Powder X-ray Diffraction (PXRD) and ^{1}H Solid-State NMR

The PXRD patterns for $Mg(OAc)_2{\cdot}4H_2O$, and α-$Mg(OAc)_2$ [Figure 1 in Supporting Information] are in good agreement with the corresponding single crystal data from Ref. 20. However, for $Mg(OAc_2){\cdot}H_2O$ the experimental pattern shows broadened peaks, particularly at low angle. This latter sample contains one or more impurities, as seen in the ^{13}C cross-polarisation (CP)MAS NMR spectra discussed later. ^{1}H MAS NMR spectra of the three targeted samples are shown in Fig. 2(a-c). For all the samples, an intense resonance at about 1.7 ppm is observed, corresponding to the methyl protons in the acetate ligands. For $Mg(OAc)_2{\cdot}4H_2O$ a second resonance is observed at 6.5 ppm, corresponding to the H_2O ligands [Fig. 2(a)]. In both the tetrahydrate and monohydrate structures, the water is directly bound as H_2O ligands as part of the octahedral coordination around the magnesium, with the respective quantities; *i.e.*, the Mg in $Mg(OAc_2){\cdot}4H_2O$ has 4 H_2O ligands, and the Mg in $Mg(OAc_2){\cdot}H_2O$ each has one H_2O ligand. In the ^{1}H NMR spectrum of $Mg(OAc_2){\cdot}H_2O$ the H_2O resonance is observed at a slightly different chemical shift of 5.9 ppm [Fig. 2(b)], reflecting the different local environment in the crystal structure. For the water-containing samples a vertical expansion to better show the water peak has been included. The intensity of this peak relative to the methyl peak is lower, which is consistent with the lower water content of the monohydrate. For α-$Mg(OAc)_2$ [Fig. 2(c)] this water signal has completely disappeared, as expected for the water-free structure of this sample. For some samples, narrow peaks present in the ^{1}H NMR spectra are from minor amounts of residual solvent. Whilst ^{1}H NMR data provides some information about the relative water content, it is not very sensitive to the more subtle differences in the local structure and coordination environments. Hence ^{13}C and ^{25}Mg NMR are used to study these materials in more detail.

Magnesium Acetate Tetrahydrate

The crystal structure of $Mg(OAc)_2{\cdot}4H_2O$ contains one crystallographically-distinct magnesium environment, and one distinct environment for the acetate group.[16] The Mg site has an octahedral local environment (MgO_6), and coordinates to four water molecules and two monodentate, terminal, acetate groups [Fig. 1]. The ^{13}C CPMAS NMR spectrum for the tetrahydrate [Fig. 2(a)] shows two narrow peaks, at 182.7 and 24.2 ppm corresponding to the two chemical environments, carbonyl and methyl groups respectively, of the acetate ligand [Table 1 in Supporting Information].

The acetate ligands participate in different bonding modes in the three targeted structures. These are summarised in Table 3 of the Supporting Information, and include terminal, bridging and chelating bonding modes. The ^{25}Mg MAS NMR spectrum for the tetrahydrate [Fig. 3(a)] shows one resonance with a characteristic second-order quadrupolar broadened lineshape with relatively moderate quadrupolar coupling, from which simulation yields a C_Q (the quadrupolar coupling constant[1,6]) of 2.5 MHz and η_Q (the quadrupolar asymmetry parameter[1,6]) of 0.74, consistent with the literature, [Table 1]. The calculated C_Q is overestimated compared to experiment, as observed previously using GIPAW NMR calculations from CASTEP data.[8,9] This could be due in part to motion arising from the four water ligands, which could be partially averaging the observed local Mg coordination environment. Discussion of possible DFT-based and sample specific issues in determining the observed NMR parameters is expanded on below in the discussion comparing the computed parameters of the hydrates to the anhydrates. The isotropic chemical shift of 3 ppm is within the known range for MgO_6 environments (approximately −15 to 26 ppm), and within a sub-range previously observed for MgO_6 with water molecule(s) in the first coordination sphere (−6.3 to 7.7 ppm).[9]

Empirical relationships are not yet well established for ^{25}Mg. However, it is useful to examine the distortion of the local environment from ideal geometry, to compare to the C_Q and to examine trends. The comparison of measures of deviation from ideal bond lengths and bond angles to C_Q values was developed by Ghose and Tsang.[23] The longitudinal strain ($|\alpha|$) is a measure of deviation from ideal bond lengths:

$$|\alpha| = \sum_i \left|\ln\left(\frac{l_i}{l_0}\right)\right| \quad (1)$$

where l_i is the individual, actual, bond lengths and l_0 is the "ideal" bond length. The ideal bond length is derived from a coordination polyhedron of the same volume as that under consideration. The shear strain ($|\psi|$) is a measure of deviation from ideal bond angles:

$$|\psi| = \sum_i |\tan(\theta_i - \theta_0)| \quad (2)$$

where θ_i and θ_0 are the actual and ideal O-Mg-O bond angles, respectively. For Mg with octahedral geometry θ_0 is 90°. For an ideal geometry, with no deviation, both $|\alpha|$ and $|\psi|$ would have a value of 0. For the discussions below, the structures obtained after DFT geometry optimisation of atomic coordinates within a fixed unit cell are used (FC), and the distortion parameters are summarised in Table 6 and Figure 5 of the Supporting Information.

In $Mg(OAc)_2 \cdot 4H_2O$ the symmetry of the octahedral environment is lowered due to the different ligands, and there is a small amount of distortion from ideal geometry. The O-Mg-O bond angles and average angles ($<\theta_{O\text{-}Mg\text{-}O}>$) are close to ideal (90 and 180°), with little deviation (standard deviation (SD) of <1), and there is only a small variation of bond length. The longitudinal strain and shear strain parameters indicate some distortion ($|\alpha|$ = 0.07, $|\psi|$ = 0.08), which in both cases are lower than for the other sites discussed in this work [Fig. 4]. With a non-zero C_Q, some distortion is expected, with the type and arrangement of the ligands a contributing factor.

Magnesium Acetate Monohydrate

The crystal structure of the $Mg(OAc)_2 \cdot H_2O$ contains two crystallographically-distinct magnesium environments, and four crystallographically-distinct acetate groups.[19] The Mg sites are both 6-coordinate (MgO_6); Mg1 coordinates to one water molecule, three monodentately bridged acetate groups and one chelating acetate group, whereas Mg2 coordinates to one water molecule, and five monodentately bridged acetate groups [Fig. 1]. Comparison of the PXRD patterns and NMR spectra indicates that none of the tetrahydrate remains after the partial dehydration process. The ^{13}C CPMAS NMR spectrum, shown in Fig. 2(b) contains sharp resonances with broader underlying components. The latter are likely to relate to non-crystalline components, such as an additional amorphous anhydrate phase.[20] Additional peaks may also relate to other partial hydration states. The calculated ^{13}C NMR data indicates that for the shifts corresponding to the monohydrate structure, the peak at higher chemical shift in the carboxyl region and the peak at lower chemical shift in the methyl region can be assigned to the chelating acetate group, and the other shifts to the bidentate groups.

The ^{25}Mg NMR spectrum for the monohydrate sample [Fig. 5(a)] is broader than that of the tetrahydrate, and shows a composite lineshape. This can be fitted using two peaks for the monohydrate and a Gaussian peak to account for an impurity [Fig. 5(b-e)] (there may be multiple low level impurities so it cannot be said if a single impurity phase produces the small additional (to the monohydrate) signals seen in the ^{13}C and ^{25}Mg NMR spectra). The ^{25}Mg NMR parameters for this fit are given in Table 1, and the simulation yields C_Q values of 5.5 and 3.9 MHz, with η_Q values of 0.4 and 0.6. The errors associated with these values can be expected to be higher due to the impurities present, causing greater uncertainty in the fitted parameters. The monohydrate was also

made by some of the authors by a different dehydration route, by partial dehydration in dry ethanol.[19] The ^{1}H, ^{13}C and ^{25}Mg MAS NMR spectra [Figure 10 in Supporting Information] are similar, also showing signs of impurities, highlighting the difficulty in preparing a pure sample of this intermediate phase.

The ^{25}Mg isotropic chemical shifts are within the known range for MgO_6[17,18], and, as for the tetrahydrate, are within the sub-range associated with coordinated water. The calculated ^{25}Mg C_Q values are again overestimated compared to experiment, and the difference between the two chemical shifts is also overestimated. However, using the DFT calculations the peak with the larger C_Q can be assigned to Mg1, and that with the smaller C_Q to Mg2.

The two crystallographically-distinct Mg environments differ slightly in the combination of coordination modes of the acetate ligands, and in their distortion from ideal octahedral geometry. For Mg1 the angles vary from ideal, with $<\theta_{O\text{-}Mg\text{-}O}>$ of approximately 160° and 90° (SD ~12). This Mg is bound by a chelating ligand, which has a strong influence on the angles around the Mg. For Mg2 bond angles are closer to ideal, with $<\theta_{O\text{-}Mg\text{-}O}>$ of approximately 175° and 90° (SD <3). Using the longitudinal strain as a measure of distortion gives $|\alpha|$ of 0.17 for Mg1 and 0.05 for Mg2. Using shear strain as a measure of distortion gives $|\psi|$ of 1.5 for Mg1 and 0.5 for Mg2. In the case of the monohydrate, it can therefore be seen that the Mg1 local environment is more distorted than for Mg2, which is consistent with the observation of a larger C_Q.

Magnesium Acetate Anhydrate

The crystal structure of the α-$Mg(OAc)_2$ contains three crystallographically-distinct magnesium environments, and six crystallographically-distinct acetate groups.[19] Two of the magnesium sites (Mg2 and Mg3) are 6-coordinated (MgO_6), and one (Mg1) is 7-coordinate (MgO_7) [Fig. 1]. Mg1 is coordinated to five monodentately bridged acetate groups and one chelating acetate group; Mg2 and Mg3 are each coordinated to six monodentately bridged acetate groups [Fig. 1]. The PXRD pattern for the sample shows good agreement to the known structure of the α-anhydrate. The ^{13}C CPMAS NMR spectrum for the anhydrate [Fig. 2(c)] shows six peaks in the carboxyl region and 4 peaks (1:1:3:1 ratio) in the methyl region. This is consistent with the six distinct acetate ligands expected from the crystal structure. Of these, one is chelating doubly bridging (chelating Mg1), the other 5 are tridentate bridging. The calculated ^{13}C isotropic chemical shifts enable partial

assignment of the ^{13}C CPMAS NMR spectrum, analogous to the situation for the monohydrate structure. One of the peaks at higher ppm in the carboxyl region (δ_{iso}^{expt} = 181.8 or 181.5 ppm) and the peak at lower ppm in the CH_3 region (δ_{iso}^{expt} = 20.9 ppm) can be assigned to the chelating ligand. The other peaks correspond to the tridentate bridging acetate groups.

The ^{25}Mg NMR spectrum [Fig. 6(a)] for the α-anhydrate is broader than the tetrahydrate, and contains a number of sharp features and broad low intensity features relating to individual peaks. The crystal structure contains three inequivalent magnesium sites so that the ^{25}Mg spectrum will be a composite of three peaks. The spectrum was fitted using the calculated ^{25}Mg NMR parameters as a starting point, and the components and simulation are shown in Fig. 6(b-e), and values, with assignment, given in Table 1. The assignment given is based on the relative quadrupolar parameters from the CASTEP calculation, which considers the periodic structure as well as the immediate local environment. A spectrum recorded at 16.4 T was used to assist in refinement of the fit. The ^{25}Mg MAS NMR spectrum can be simulated with three peaks, in agreement with the three sites in the crystal structure, and yields C_Qs of 5.0, 5.4, and 1.4 MHz with η_Qs of 0.5, 0.8, and 0.7. The calculated C_Qs are less overestimated compared to experiment than for the hydrates, and they enable the three peaks to be assigned to the crystallographic sites. These comprise two with large C_Qs (Mg1 and Mg2) and one with a small C_Q (smaller than observed for $Mg(OAc)_2{\cdot}4H_2O$; (Mg3)). The integrated intensities of each of the three lines is approximately equal, as expected from there being the same number of magnesiums in each coordination within this structure. The isotropic chemical shifts for the two MgO_6 sites (Mg2 and Mg3) are within or close to the known range for such coordinations. The isotropic chemical shift of the MgO_7 site is of particular interest as trends in shift for coordination numbers is a useful characterisation tool. However, in this case the shift for Mg1 is within the range defined for MgO_6, and therefore assignment of coordination number cannot be made based on shift alone.

To try to understand the variation of C_Qs measured for α-$Mg(OAc)_2$, the distortion of the local Mg environments can be examined. Mg2 deviates from ideal octahedral geometry with $<\theta_{O\text{-}Mg\text{-}O}>$ of 170° (SD 4) and 90° (SD 8). The distortion measures for this site are $|\alpha|$ 0.09 and $|\psi|$ 1.2, which are similar to Mg1 of $Mg(OAc_2){\cdot}H_2O$, and indeed they exhibit similar C_Q values. Mg3 of α-$Mg(OAc)_2$, displays remarkably similar distortion considering the considerably lower C_Q, with $<\theta_{O\text{-}Mg\text{-}O}>$ of 169°

(SD 4) and 90° (SD 9), and with $|\alpha|$ of 0.12 and $|\psi|$ of 1.4. In Fig. 4 the distortion measures $|\alpha|$ and $|\psi|$ are plotted against calculated and experimental C_Q values, for the three known $Mg(OAc)_2 \cdot xH_2O$ (x = 0, 1, 4) structures. In each case, Mg3 of α-$Mg(OAc)_2$ is a clear outlier, with the other MgO_6 sites showing a global trend of increasing C_Q with increasing distortion. Mg1 of the α-anhydrate, the MgO_7 site, is pentagonal bipyramidal (ideal angles 72, 90°). The average angles are close to ideal, but with high level of variation, $<\theta_{O\text{-}Mg\text{-}O}>$ 74° (SD 9.5) and 90° (SD 11), and the shear strain is 2.5. Mg1 is bound by the chelating ligand, which constrains some of the angles. This distortion is reflected in the large C_Q for this site. The lack of a defining quantitative measure, may indicate that these distortion parameters poorly describe the local magnesium environment, and there may be other longer-range contributing factors, or that an alternative approach to analyse the local environment is needed

Another way to consider the local environments, to provide insight into the NMR parameters, is to use a qualitative approach and consider the bonding modes and arrangement of the acetate ligands (Table 3 and Figure 6 in the Supporting Information). For α-$Mg(OAc)_2$, these indicate some symmetry in the arrangement of bonding types, although distortion is present in the geometry (bond lengths and angles). Mg2 has the least symmetric arrangement (largest C_Q), then Mg1, and Mg3 has the most symmetric arrangement (smallest C_Q). This approach can also be used to compare the two magnesium sites in $Mg(OAc_2)\cdot H_2O$, where Mg2 has higher symmetry in the arrangement of the ligand bonding modes, and has the lower value of C_Q.

An examination of the change in the Mg-O bond lengths and O-Mg-O bond angles after geometry optimisation is given in Figures 7 and 8 of the Supporting Information. The MgO_x in the α-anhydrate structure undergo less change in geometry, than in the tetrahydrate and monohydrate structures and the calculated C_Q values are also a closer match [Figure 9 of the Supporting Information]. The calculated C_Q values for those structures with water ligands, with smaller structural units – individual octahedral $[Mg(OAc_2)\cdot 4H_2O]$ and chains $[Mg(OAc_2)\cdot H_2O]$, have a greater overestimation. The structure of the α-anhydrate has a more rigid 3D network of polyhedra. This suggests that structural contributions are significant in the differences observed between calculated and experimental C_Q values for the hydrated phases.

The effective coordinations and Bond Valence Sums were obtained from VESTA[24], and are given in Table 7 of the Supporting Information. Analysis of the coordination of Mg1 in α-$Mg(OAc)_2$, gives an effective coordination of 6.6 and Bond Valence Sum (BVS) of 1.8 (for Mg2 and Mg3, effective coordinations are 5.9 and 5.9, with BVSs of 2.1 and 2.2 respectively). The Mg-O bond lengths of the two chelating branches are 2.27 and 2.32 Å, before geometry optimisation and 2.27 and 2.34 Å after geometry optimisation. The effective bond coordination is similarly reduced from a perfect polyhedron for the chelated Mg of the monohydrate (5.7, MgO_6 environment), which has a BVS of 2.1, and Mg-O bond lengths of 2.19 and 2.19 Å before geometry optimisation and 2.19 and 2.22 Å after. Whilst the chelating ligand of the MgO_7 site in α-$Mg(OAc)_2$ may be considered to be tethered in place by its coordination to a different Mg site, it does influence the arrangement of the remaining ligands and contributes to the effective coordination. Therefore the coordination of Mg1 of α-$Mg(OAc)_2$ may certainly be described nominally as MgO_7.

During the course of this work, several attempts to synthesise the α-anhydrate led to the unexpected formation of a second phase. The PXRD pattern in Figure 2 of the Supporting Information shows a resemblance to the pattern for a little studied second anhydrate phase.[20,21] The additional peaks in the PXRD pattern do not relate to the α-anhydrate or the monohydrate or tetrahydrate, and therefore relate to an unidentified impurity. The crystal structure of the β-anhydrate has not yet been determined; however, NMR data can provide structural insight. Whilst synthesis routes for both α- and β-$Mg(OAc)_2$ were reported in the literature in 1959,[21] the crystal structure for the α-phase was not determined until 2012, from a sample formed by dehydrating the tetrahydrate,[19] and recent reporting of the β-phase has been in a mixture with the α-phase after thermal dehydration of the tetrahydrate.[20] The NMR spectra for this sample are different to those of the previously discussed anhydrate and hydrate phases, highlighting the clear structural differences between the β-anhydrate and the other known phases. The ^1H MAS NMR spectrum is dominated by a peak at 1.8 ppm, for the acetate ligand, confirming that water has not infiltrated the synthesis [Fig. 2(d)]. Low intensity impurity peaks are also present. The ^{13}C CPMAS NMR spectrum, shown in Fig. 2(d), is more complex than the α-anhydrate discussed above. While the structure is unknown, PXRD measurements have indicated that the β-anhydrate structure has lower triclinic symmetry than the α-anhydrate phase which is orthorhombic,[19] and it is also possible that impurities are present, as the synthesis was not tailored to this phase.[19]

The ^{25}Mg MAS NMR spectrum shown in Fig. 7(a), is broader than the tetrahydrate, but narrower than the α-anhydrate, and shows distinct features indicating a composite of second-order quadrupolar broadened lineshapes. This phase was synthesised with ^{25}Mg enrichment, which enabled acquisition of a STMAS spectrum [Fig. 7(b)]. The spectrum unambiguously reveals four distinct magnesium lineshapes, and therefore four corresponding local environments. These comprise one lineshape with a C_Q of approximately 1.8 MHz and η_Q of 0.6, and three with C_Qs of approximately 3.1 MHz with η_Q from 0.47 to 1. The former set of parameters is similar to that obtained for Mg3 of the α-anhydrate. The ^{25}Mg isotropic chemical shifts are consistent with MgO_6 local environments for all of the magnesium sites. MgO_6 is considered most likely, as MgO_7 is more unusual, and cannot be ruled out. Although the STMAS NMR spectrum is not strictly quantitative, the integrated intensity ratio of the four resonances is approximately 1:1:1:1, which suggests that the relative populations of the four sites are similar, particularly for those with similar C_Q values. Therefore the ^{25}Mg NMR data provide several important structural constraints and any future crystal structure of the β-anhydrate phase will need to be consistent with this data. However, given that impurities have been identified by PXRD and ^{1}H and ^{13}C MAS NMR spectra, even if they contained magnesium they are unlikely to produce significant intensity and the approximately equal strongly suggests all the signals come from the same phase.

Conclusions

In this work, distinct ^{25}Mg MAS NMR spectra were obtained at natural abundance for $Mg(OAc)_2{\cdot}4H_2O$, $Mg(OAc)_2{\cdot}H_2O$, and α-$Mg(OAc)_2$, and with ^{25}Mg enrichment for β-$Mg(OAc)_2$. From these, ^{25}Mg NMR parameters were obtained for a range of MgO_6 environments and for a MgO_7 environment, therefore, expanding the data available for this isotope. ^{25}Mg enrichment enabled the acquisition of a high quality 2D STMAS spectrum within 21 hrs, which provided insight into this second $Mg(OAc)_2$ phase, for which a crystal structure is not available. The ^{1}H MAS NMR spectra clearly reflect the decreasing water content in going from the tetrahydrate to the α-anhydrate. The ^{13}C MAS NMR spectra provide information on the number of distinct acetate ligands, and insight into their bonding modes.

Whilst CASTEP overestimates ^{25}Mg C_Q values, it is still a useful aid in simulating experimental data, particularly in providing constraints for superimposed signals, and assignment to crystallographic sites. Consideration of the overestimation observed by Cahill *et al.* (C_Q^{calc} = 1.225C_Q^{exp} – 0.13 (in MHz)) brings the calculated C_Q values into much closer agreement with experimental ones.[8] The ^{25}Mg isotropic chemical shifts for the MgO_6 sites fall within or close to the known range, with those sites containing water in the first coordination sphere located within a sub-range previously observed for such sites.[17,18] However, the ^{25}Mg isotropic chemical shift for the MgO_7 site also falls within the MgO_6 range, indicating that caution must be taken when assigning coordination number of MgO_x sites based solely on the chemical shift. A lack of discernible trends between distortion measures and ^{25}Mg NMR parameters indicate that factors beyond the local geometry are contributing to the observed NMR parameters.

This work shows that ^{25}Mg solid-state NMR can be sensitive to the hydration state of the sample, by reflecting the local environments present in the structures. In the hydrated samples, water acts as a ligand, alongside acetate groups, thereby directly influencing the local environment. Whereas in the anhydrate samples, only acetate ligands are present, enabling different local environments and 3D structures to be formed.

Experimental: Materials and Methods

Materials

Magnesium acetate tetrahydrate ($Mg(OAc)_2{\cdot}4H_2O$) was obtained from Sigma Aldrich (≥99%). Different synthesis routes were utilised to produce samples of the monohydrate and anhydrate for analysis, using either $Mg(OAc)_2{\cdot}4H_2O$ or MgO as the starting material. The use of the latter enables ^{25}Mg enrichment *via* ^{25}MgO (Cortecnet, 99.2%). Generally, the synthesis approach for enriched samples was small scale (using approx. 29 mg of MgO), due to the high cost of ^{25}MgO. Magnesium acetate anhydrate (α-$Mg(OAc)_2$) was prepared according to the procedure of Walter-Levy *et al.*,[21] using MgO, acetic acid and ethyl acetate. The sample was phase pure by PXRD and ^{13}C solid-state NMR. In later attempts to synthesise the α-anhydrate a different product was obtained, β-$Mg(OAc)_2$, which is discussed in the results section. Magnesium acetate monohydrate ($Mg(OAc_2){\cdot}H_2O$) was prepared by partial dehydration of $Mg(OAc)_2{\cdot}4H_2O$, by heating to approximately 120 °C for 1 hr, under quasi-sealed conditions, [based on Ref. 21] using a 25 mL flask

and a rubber stopper containing a syringe needle. In another preparation magnesium acetate monohydrate was obtained by partial dehydration of $Mg(OAc)_2{\cdot}4H_2O$ in dried ethanol as described in Ref. 25.

Magnesium acetate phases are hygroscopic, so samples were kept in a glove box to maintain their prepared hydration state, including $Mg(OAc)_2{\cdot}4H_2O$. Of the materials studied, $Mg(OAc)_2{\cdot}4H_2O$, $Mg(OAc)_2{\cdot}H_2O$, and α-$Mg(OAc)_2$ contained natural abundance ^{25}Mg, whereas β-$Mg(OAc)_2$ was ^{25}Mg enriched.

Characterisation Methods

Powder X-Ray Diffraction

Laboratory X-ray powder diffraction of samples was performed on a Rigaku SmartLab instrument, using a 9 kW Cu-source generator. Due to the sensitivity of the samples to moisture, samples were prepared in either a capillary tube sealed with grease, or in a sealed cell. Typically, 6° to 70° 2θ ranges were investigated over 1 to 2 hrs for the former sample holder, and 6° to 90° 2θ ranges were investigated over 3 hrs, for the latter, with a step size of 0.01°.

Solid-state NMR

^{11}H, ^{13}C and ^{25}Mg solid-state NMR spectra were obtained at 16.4 T on a Bruker Avance III 700 MHz spectrometer operating at Larmor frequencies of 700.1, 176.0, and 42.9 MHz, respectively. Powdered samples were packed into 4 or 2.5 mm MAS rotors, and rotated at MAS rates of 10 kHz for ^{13}C, 12.5 kHz for ^{25}Mg, and 25 kHz for ^{1}H. ^{13}C MAS NMR spectra were acquired using cross-polarisation (CP), with a contact pulse (ramped for ^{1}H) of 1 ms and ^{1}H decoupling (TPPM)[26] applied throughout acquisition. A recycle delay of 5 s was used for ^{1}H and ^{13}C experiments. ^{1}H MAS NMR spectra were recorded using a depth pulse sequence.[27] ^{25}Mg MAS NMR spectra were acquired using a Hahn echo (90°-τ-180°-τ), with ^{1}H decoupling, using a 2 s recycle delay.

^{25}Mg solid-state NMR spectra were also obtained at 20.0 T on a Bruker Avance 850 MHz spectrometer operating at a Larmor frequency of 52.0 MHz. Powdered samples were packed into 4 mm MAS rotors and a conventional HX low-gamma Bruker MAS probe was used. A MAS rate of 14 kHz was used, with a recycle delay of 2 s. 1D MAS NMR spectra were acquired using a Hahn echo, with ^{1}H decoupling, and a double frequency sweep (DFS) sequence[28] was integrated into the pulse

sequence to enhance the signal sensitivity. The enhancement achieved by DFS is expected to be relatively uniform for similar C_Qs, and therefore the relative intensities of the peaks in the spectra should be approximately quantitative.[29]

The two-dimensional ^{25}Mg STMAS spectrum[22,30-32] was recorded using a phase-modulated split-t_1 pulse sequence, with ^{1}H decoupling (TPPM)[26] and a recycle interval of 2 s. A double-quantum filter was also used in the STMAS experiment to ensure the removal of the undesirable autocorrelation diagonal.[33] Prior to the ^{25}Mg STMAS experiment, for which high accuracy of the magic angle is required to be effective, rubidium sulphate was used to set the spinning axis. After setting the magic angle, the sample was carefully changed using the Bruker pneumatic insert-eject system, with a low flow of gas to cushion the rotor during its insertion.

^{13}C and ^{1}H MAS NMR spectra (10 kHz MAS, 16.4 T) were run before and after the ^{25}Mg experiments and showed no phase change as a result of spinning the samples for lengthy periods, indicating that the water remains bound to the magnesium. The rotors were also packed in a glove box under N_2, and remain well sealed, preventing water from affecting the anhydrate phases. NMR spectra were calibrated using the secondary standards MgO (26 ppm) for ^{25}Mg and L-alanine for both ^{1}H (NH_3 = 8.5 ppm) and ^{13}C (CH$_3$ = 20.5 ppm). Spectral fitting and simulations of one-dimensional MAS NMR spectra were performed using Bruker TopSpin 3.2 and Dmfit.[34]

DFT calculations

Calculations of NMR parameters were carried out using the CASTEP code (8.0 Academic Release)[35-38], employing the GIPAW algorithm,[36] to reconstruct the all-electron wave function in the presence of a magnetic field. Calculations were performed on Lancaster University's High End Computer (HEC) cluster, using the GGA PBE functional, with core-valence interactions described by ultrasoft pseudopotentials,[37] which were generated on-the-fly. A plane-wave energy cut-off of 50 Ry (~680 eV) was used, and integrals over the Brillouin zone were performed using a *k*-point spacing of 0.04 Å^{-1}. The convergence of total energy and calculated NMR parameters with respect to k-point spacing and energy cut-off was checked using $Mg(OAc)_2{\cdot}4H_2O$. The ^{1}H and ^{13}C isotropic shielding was converged to within 0.01 ppm, while the ^{25}Mg isotropic shielding was converged to within 1 ppm and the C_Q to within 0.001 MHz. Structural parameters, atomic positions and unit-cell parameters, were obtained from experimental crystal structures.[19] Different geometry

optimisation procedures were explored, including optimising the atomic coordinates with a fixed unit cell (FC), allowing the unit cell to vary (RC), and using dispersion correction schemes (TS). For the latter, dispersive interactions were reintroduced using the scheme of Tkatchenko and Scheffler,[39] as implemented by McNellis *et al*.[40] From comparison of calculated and experimental ^{1}H and ^{13}C NMR parameters it is clear that some form of geometry optimisation is required. It is well known that H atom locations are less accurate from XRD data. Similar structures and therefore NMR parameters were obtained for the different geometry optimisation methods, and those from the fixed unit cell method are discussed in the text. The calculated ^{13}C and ^{25}Mg NMR parameters are given in the Tables 1 and 4 of the Supporting Information, and comparison of MgO_x local environments in Figures 7 and 8 of the Supporting Information. The isotropic chemical shift, δ_{iso}, is given by $-(\sigma_{iso} - \sigma_{ref})$, where σ_{iso} is the isotropic shielding and σ_{ref} is a reference shielding. For ^{13}C, plots of the computed σ_{iso}, against experimental δ_{iso} for $Mg(OAc)_2{\cdot}4H_2O$ and α-$Mg(OAc)_2$ (from fixed unit cell geometry optimisations) were used to obtain σ_{ref} (Figure 3 of the Supporting Information). This provided a reference shielding of σ_{ref} 174.5 ppm for ^{13}C. For ^{25}Mg, a satisfactory σ_{ref} was not obtained and therefore the σ_{iso} are reported. NMR parameters were calculated for the same structures using PBEsol instead of PBE. The calculated NMR parameters are similar for the PBE and PBEsol data (Figure 4 of the Supporting Information), except for the ^{25}Mg σ_{iso}, this suggests a DFT issue for this parameter.

Acknowledgements

Lancaster University is thanked for provision of the NMR, XRD and HEC facilities, and for partially funding this research. Characterisation facilities were part funded by the European Regional Development Fund (ERDF) under the Collaborative Technology Access Program (cTAP). Dr Nathan Halcovitch (Lancaster University) is gratefully acknowledged for providing synthesis and XRD support. The UK 850 MHz solid-state NMR Facility used in this research was funded by EPSRC and BBSRC (contract reference PR140003), as well as the University of Warwick including via part funding through Birmingham Science City Advanced Materials Projects 1 and 2 supported by Advantage West Midlands (AWM) and the European Regional Development Fund (ERDF). JVH also acknowledges the University of Warwick Scientific Computing Research Technology Platform (RTP), and EPSRC grant EP/K000128/1, for access to the TINUS and MINERVA high performance computing

clusters, respectively, that facilitated a component of the computational effort undertaken in this work.

Key words: local structure, magnesium acetates, magnesium-25, solid state NMR, STMAS

References

[1] K. J. D. MacKenzie, M. E. Smith, *Multinuclear solid-state NMR of inorganic materials*, Pergamon Press, **2002**.

[2] J. V. Hanna, M. E. Smith, *Solid State Nucl. Magn. Reson.* **2010**, *38*, 1-18. DOI: 10.1016/j.ssnmr.2010.05.004

[3] T. Charpentier, *Solid State Nucl. Magn. Reson.* **2011**, *40*, 1-20. DOI: 10.1016/j.ssnmr.2011.04.006

[4] C. Bonhomme, C. Gervais, F. Babonneau, C. Coelho, F. Pourpoint, T. Azais, S. E. Ashbrook, J. M. Griffin, J. R. Yates, F. Mauri, C. J. Pickard, *Chem. Rev.* **2012**, *112*, 5733-5779. DOI: 10.1021/cr300108a

[5] S. E. Ashbrook, D. McKay, *Chem. Comm*. **2016**, *52*, 7186-7204. DOI: 10.1039/c6cc02542k

[6] M. E. Smith, E. R. H. van Eck, *Prog. Nucl. Magn. Reson. Spectrosc.* **1999**, *34*, 159-201. DOI: 10.1016/S0079-6565(98)00028-4

[7] R. Dupree, M. E. Smith, *Chem. Comm.* **1988**, 1483-1485. DOI: 10.1039/c39880001483

[8] L. S. Cahill, J. V. Hanna., A. Wong, J. C. C. Freitas, J. R. Yate, R. K. Harris, M. E. Smith, *Chem. Eur. J.* **2009**, *15*, 9785-9798. DOI: 10.1002/chem.200900346

[9] P. J. Pallister, I. L. Moudrakovski, J. A. Ripmeester, *Phys. Chem. Chem. Phys.* **2009**, *11*, 11487-11500. DOI: 10.1039/b916076k

[10] J. M. Griffin, A. J. Berry, S. E. Ashbrook, *Solid State Nucl. Magn. Reson.* **2011**, *40*, 91-99. DOI: 10.1016/j.ssnmr.2011.08.004

[11] J. M. Griffin, A. J. Berry, D. J. Frost, S. Wimperis, S. E. Ashbrook, *Chem. Sci.* **2013**, *4*, 1523-1538. DOI: 10.1039/C3SC21892A

[12] K. Shimoda, T. Nemoto, K. Saito, *J. Phys. Chem. B* **2008**, *112*, 6747-6752. DOI: 10.1021/jp711417t

[13] G. Scholz, D. Heidemann, E. Kemnitz, *Z. Anorg. Allg. Chem.* **2013**, *639*, 694-701. DOI: 10.1002/zaac.201200554

[14] J. Xu, V. V. Terskikh, Y. Huang, *J. Chem. Phys. Lett.* **2013**, *4*, 7-11. DOI: 10.1021/jz301954t

[15] J. Xu, B.E.G. Lucier, R. Sinelnikov, V. V. Terskikh, V. N. Staroverov, Y. Huang, *Chem. Eur. J.* **2015**, *21*, 14348-14361. DOI: 10.1002/chem.201501954

[16] J. Xu, E. S. Blaakmeer, A. S. Lipton, T. M. McDonald, Y. M. Liu, B. Smith, J. R. Long, A. P. M. Kentgens, J. R. Reimer, *J. Phys. Chem. C* **2017**, *121*, 19938-19945. DOI: 10.1012/acs.jpcc.7b7809

[17] J. C. C. Freitas, M. E. Smith, *Ann. Rep. NMR Spectrosc.* **2012**, *75*, 25-114. DOI: 10.1016/B978-0-12-397018-3.00002-8

[18] I. L. Moudrakovski, *Ann. Rep. NMR Spectrosc.* **2013**, *79*, 129-240. DOI: 10.1016/B978-0-12-408098-0.00004-5

[19] K. Scheurell, R. König, S. I. Troyanov, E. Kemnitz, *Z. Anorg. Allg. Chem.* **2012**, *638*, 1265-1273. DOI: 10.1002/zaac.201200269

[20] N. Koga, Y. Suzuki, T. Tatsuoka, *J. Phys. Chem. B* **2012**, *116*, 14477-14486. DOI: 10.1021/jp3052517

[21] L. Walter-Levy, I. Soleilhavoup, P. M. de Wolff, *Compt. rend.* **1959**, *249*, 1234-1236.

[22] S.E. Ashbrook, S. Wimperis, *Prog. Nucl. Magn. Reson. Spectrosc.* **2004**, *45*, 53–108. DOI: 10.1016/j.pnmrs.2004.04.002

[23] S. Ghose, T. Tsang, *Am. Mineral*, **1973**, *58*, 748-755.

[24] K. Momma, F. Izumi, *J. Appl. Crystallogr.* **2011**, *44*, 1272-1276. DOI: 10.1107/S0021889811038970

[25] K. Isa, M. Nogawa, *Thermochim. Acta* **1984**, *75*, 197. DOI: 10.1016/0040-6031(84)85020-0

[26] A. E. Bennett, C. M. Rienstra, M. Auger, K. V. Lakshmi, R. G. Griffin, *J. Chem. Phys.* **1995**, *103*, 6951−6958. DOI: 10.1063/1.470372

[27] D. G. Cory, W. M. Ritchey, *J. Magn. Reson.* **1988**, *80*, 128-132. DOI: 10.1016/0022-2364(88)90064-9

[28] A. P. M. Kentgens, R. Verhagen, *Chem. Phys. Lett.* **1999**, *300*, 435–443. DOI: 10.1016/S0009-2614(98)01402-X

[29] D. Iuga and A. P.M. Kentgens, *J. Magn. Reson.* **2002**, 158, 65-72. DOI: 10.1016/S1090-7807(02)00061-7

[30] Z. Gan, *J. Am. Chem. Soc.* **2000**, *122*, 3242-3243. DOI: 10.1021/ja9939791

[31] J. Amoureux, C. Fernandez, L. Frydman, *Chem. Phys. Lett.*, **1996**, *259*, 347-355. DOI: 10.1016/0009-2614(96)00809-3

[32] N. G. Dowell, S. E. Ashbrook, S. Wimperis, *J. Phys. Chem. B* **2004**, *108*, 13292-13299. DOI: 10.1021/jp047868m

[33] H. T. Kwak, Z. Gan, *J. Magn. Reson.*, **2003**, *164*, 369-372. DOI: 10.1016/S1090-7807(03)00246-5

[34] D. Massiot, F. Fayon, M. Capron, I. King, S. Le Calvé, B. Alonso, J. O. Durand, B. Bujoli, Z. Gan, G. Hoatson, *Magn. Reson. Chem.* **2002**, *40*, 70-76. DOI: 10.1002/mrc.984

[35] S. J. Clark, M. D. Segall, C. J. Pickard, P. J. Hasnip, M. J. Probert, K. Refson, M. C. Payne, **2005**, *220*, 567-570. DOI: 10.1524/zkri.220.5.567.65075

[36] C. J. Pickard, F. Mauri, *Phys. Rev. B: Condens. Matter Mater. Phys.* **2001**, *63*, 245101. DOI: 10.1103/PhysRevB.63.245101

[37] J. R. Yates, C. J. Pickard, F. Mauri, *Phys. Rev. B: Condens. Matter Mater. Phys.* **2007**, *76*, 024401. DOI: 10.1103/PhysRevB.76.024401

[38] M. Profeta, F. Mauri, C. J. Pickard, *J. Am. Chem. Soc.* **2003**, *125*, 541. DOI: 10.1021/ja027124r

[39] A. Tkatchenko, M. Scheffler, *Phys. Rev. Lett.*, **2009**, *102*, 073005. DOI: 10.1103/PhysRevLett.102.073005

[40] E. R. McNellis, J. Meyer, K. Reuter, *Phys. Rev. B: Condens. Matter Mater. Phys.* **2009**, *80*, 205414. DOI: 10.1103/PhysRevB.80.205414

Figure Captions

Figure 1: Local magnesium environments for $Mg(OAc)_2{\cdot}4H_2O$, $Mg(OAc)_2{\cdot}H_2O$ and α-$Mg(OAc)_2$.

Figure 2: ^{1}H MAS NMR spectra (16.4 T, 25 kHz MAS) and ^{13}C CPMAS NMR spectra (16.4 T, 12.5 kHz MAS) of (a) magnesium acetate tetrahydrate, (b) magnesium acetate monohydrate, (c) α-magnesium acetate anhydrate, and (d) β-magnesium acetate anhydrate. ^{1}H NMR spectra are the result of averaging (a) 512, (b) 256 and (c,d) 128 transients, with a recycle interval of 5 s. ^{13}C CPMAS NMR spectra are the result of averaging (a) 1136, (b) 20000, (c) 2528, and (d) 14944 transients, with a recycle interval of 5 s. Vertical expansions of the water peaks in the ^{1}H NMR spectra of (a) and (b) are shown. Horizontal expansions of the ^{13}C NMR spectra are included to show the peaks in more detail.

Figure 3: (a) ^{25}Mg MAS NMR spectrum (16.4 T, 12.5 kHz MAS) of magnesium acetate tetrahydrate, with (b) a simulation. The spectrum is the result of averaging 128720 transients, with a recycle interval of 2 s.

Figure 4: Plots of distortion measures, (a,b) longitudinal strain, $|\alpha|$, and (c,d) shear strain, $|\psi|$, versus (a,c) calculated and (b,d) experimental ^{25}Mg C_Q for the phases with known crystal structure.

Figure 5: (a) ^{25}Mg MAS NMR spectrum (20.0 T, 14 kHz MAS) of magnesium acetate monohydrate, with (b) a simulation and (c,d,e) the individual components. The spectrum is the result of averaging 28192 transients, with a recycle interval of 2 s. Lorentzian line broadening was applied.

Figure 6: (a) ^{25}Mg MAS NMR spectra (20.0 T, 14 kHz MAS) of α-magnesium acetate anhydrate, with (b) a simulation and (c,d,e) the individual components. The spectrum is the result of averaging 40224 transients, with a recycle interval of 2 s. For (d) an inset is also shown so that the lineshape can be more clearly seen. Lorentzian line broadening was applied.

Figure 7: ^{25}Mg MAS and 2D STMAS NMR spectra (20.0 T, 14 kHz MAS) of ^{25}Mg-enriched β-magnesium acetate anhydrate, (a) and (b) respectively. Figure includes a sum projection shown in (b) and cross-sections extracted from the 2D spectrum, with fits, shown in (c). (d) is a 1D simulation using the extracted values from (c). The 1D MAS spectrum is the result of averaging 3184 transients, with a recycle interval of 2 s. The 2D spectrum is the result of average 512 transients for each increment.

Figures

Figure 1

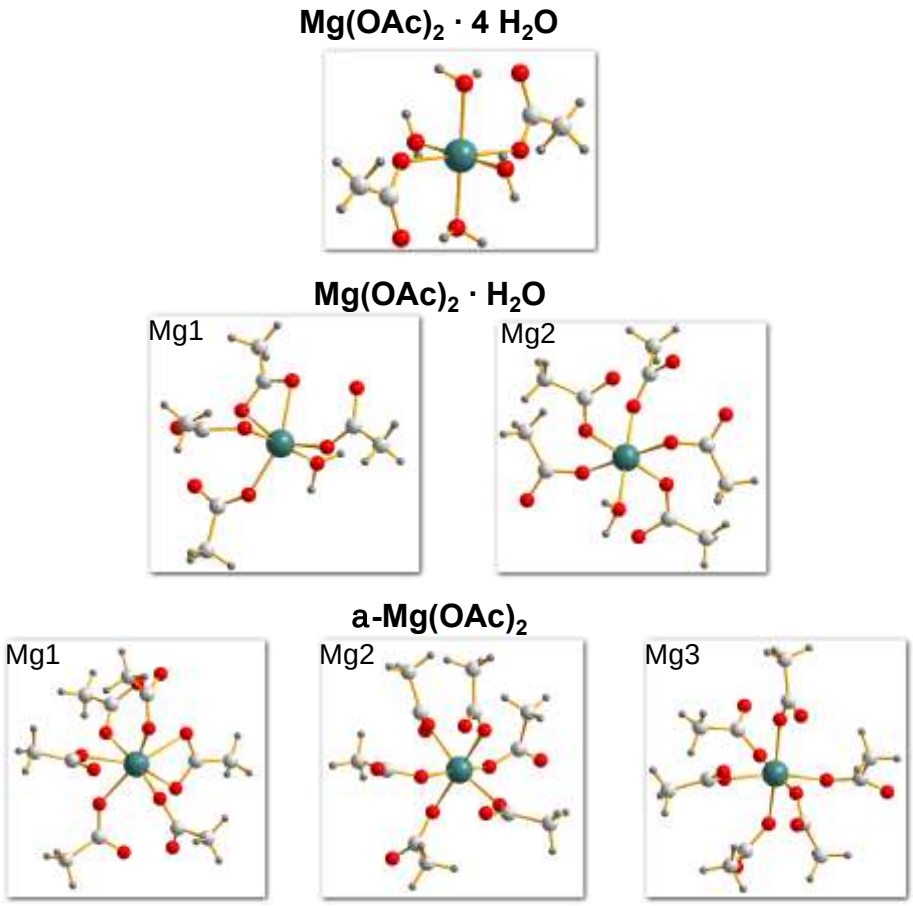

Figure 2

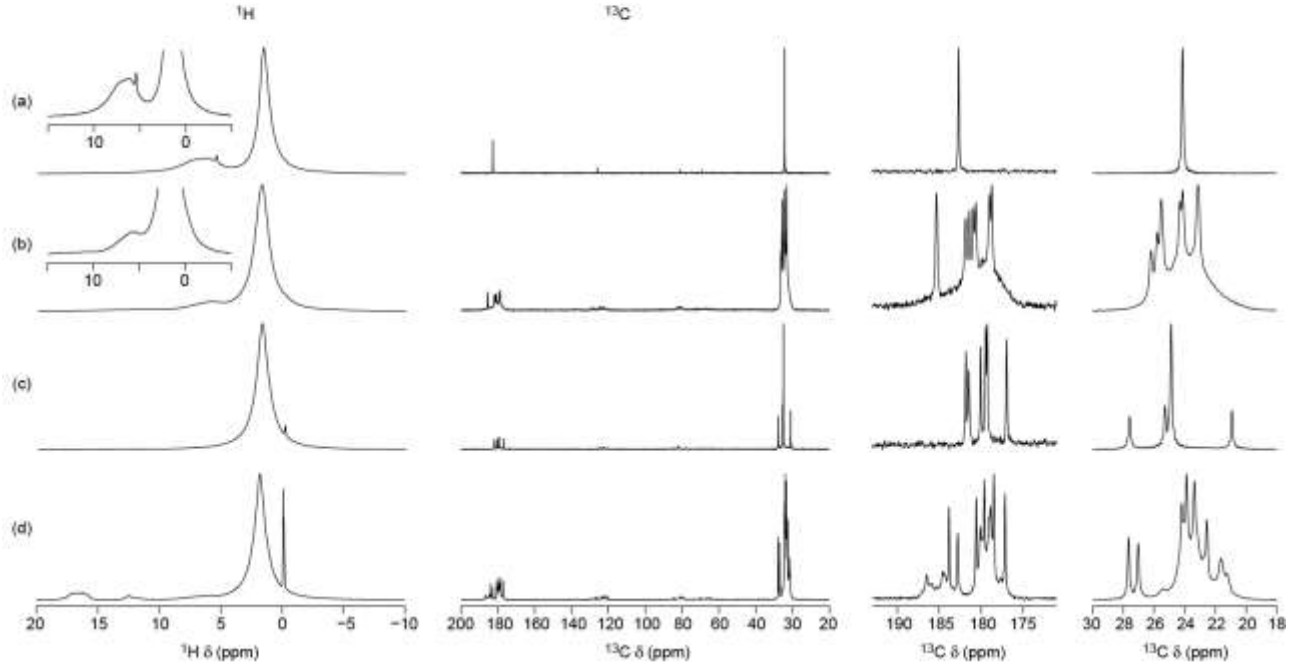
^{1}H
^{13}C
(a)
(b)
(c)
(d)
10
0
20 15 10 5 0 −5 −10
^{1}H δ (ppm)
200 180 160 140 120 100 80 60 40 30 20
^{13}C δ (ppm)
190 185 180 175
^{13}C δ (ppm)
30 28 26 24 22 20 18
^{13}C δ (ppm)

Figure 3

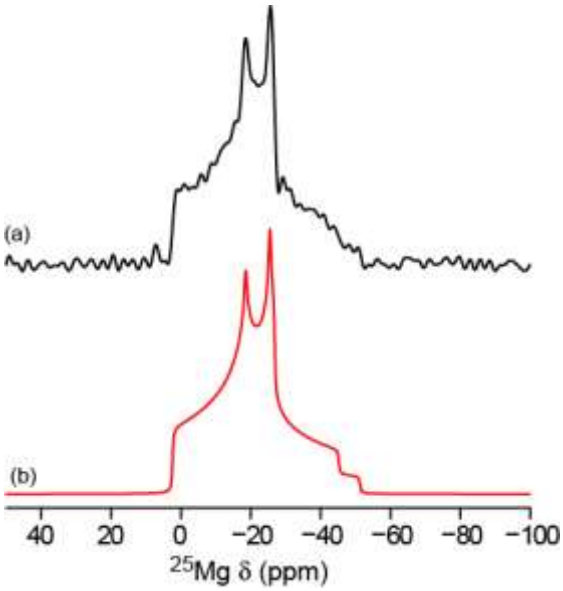

Figure 4

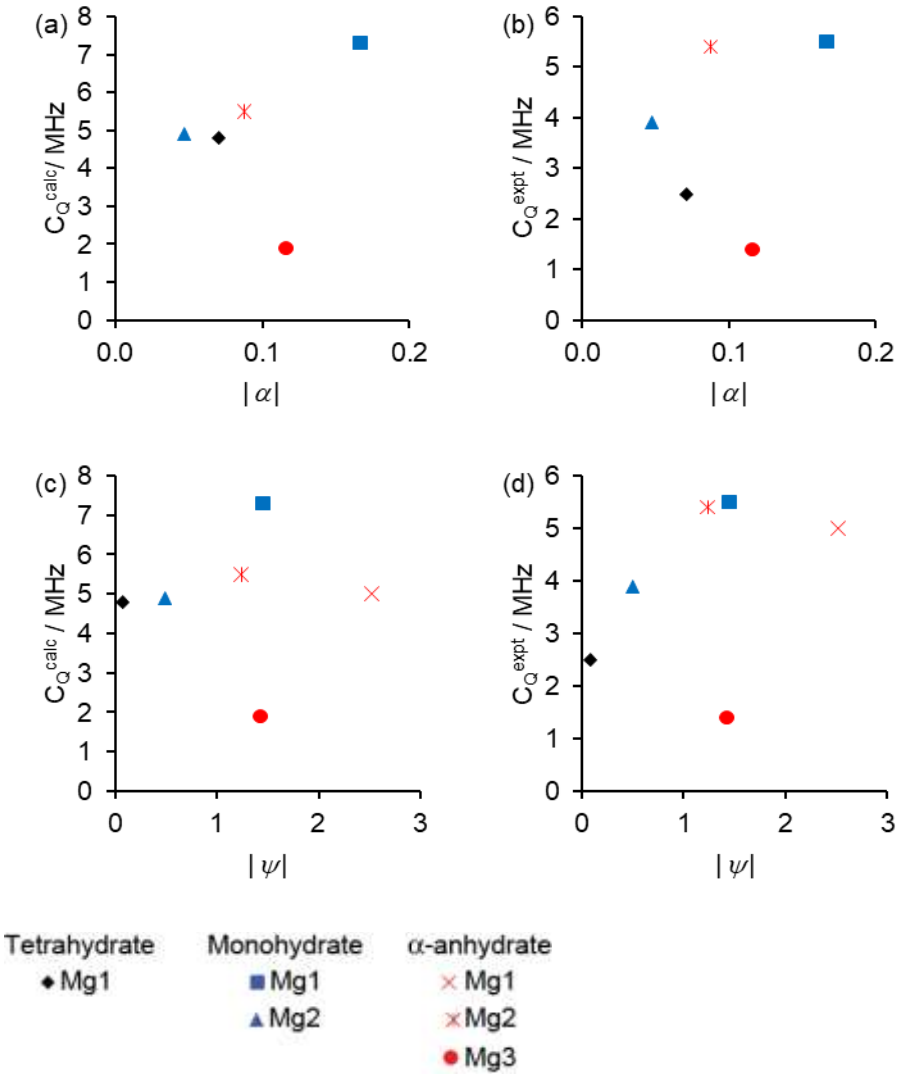
(a)
(b)
(c)
(d)
C_Q^{calc} / MHz
C_Q^{expt} / MHz
|α|
|ψ|
Tetrahydrate
Mg1
Monohydrate
Mg1
Mg2
α-anhydrate
Mg1
Mg2
Mg3

Figure 5

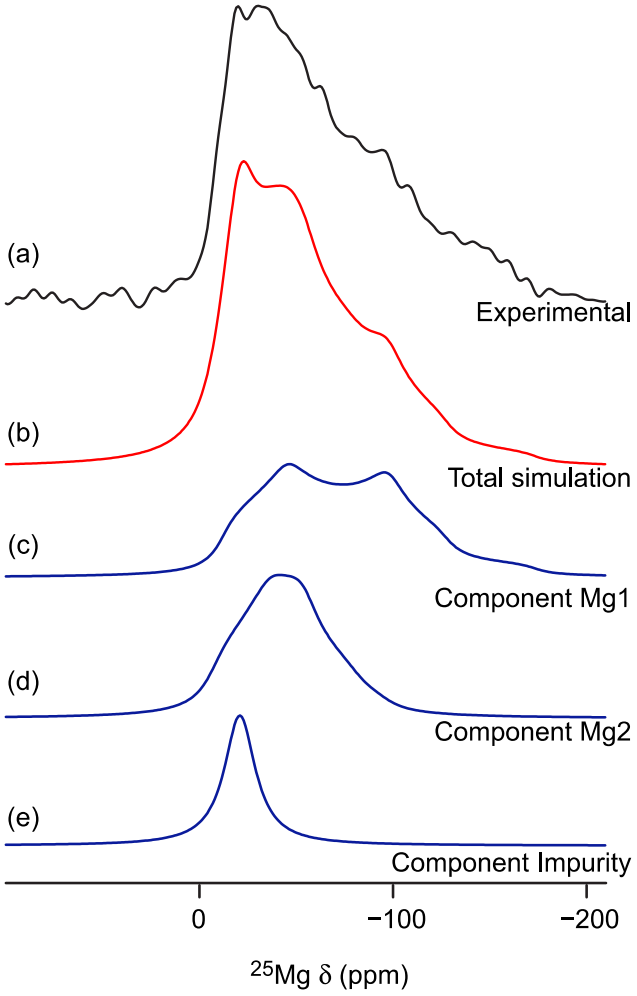
(a)
Experimental
(b)
Total simulation
(c)
Component Mg1
(d)
Component Mg2
(e)
Component Impurity
0
−100
−200
25Mg δ (ppm)

Figure 6

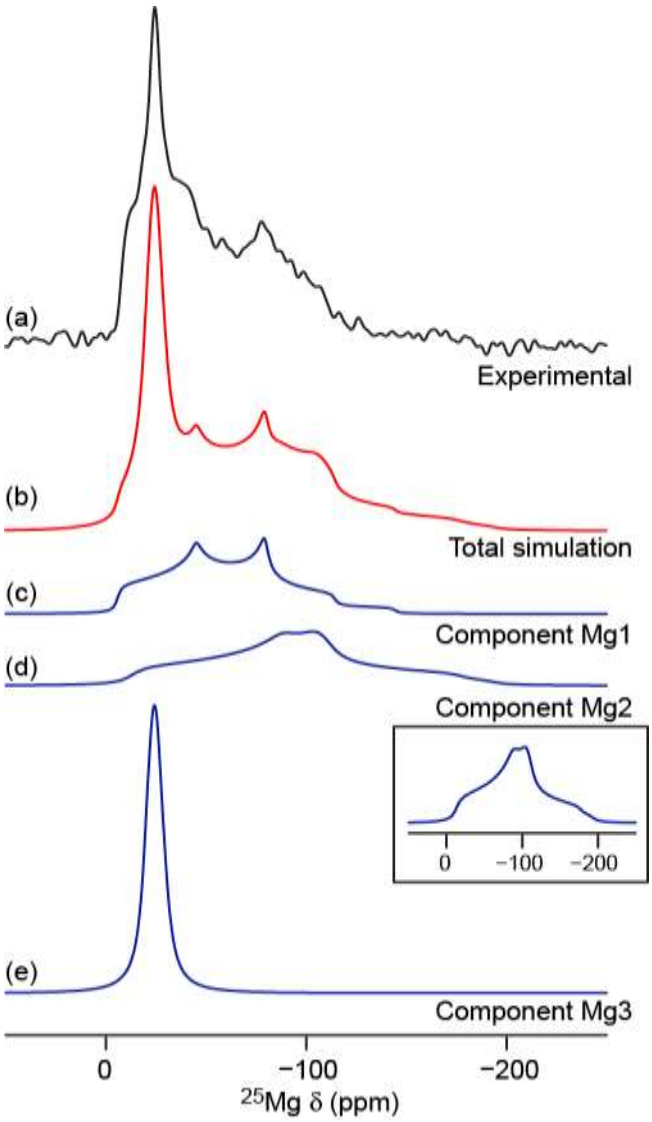
(a)
Experimental
(b)
Total simulation
(c)
Component Mg1
(d)
Component Mg2
0
−100
−200
(e)
Component Mg3
0
−100
−200
25Mg δ (ppm)

Figure 7

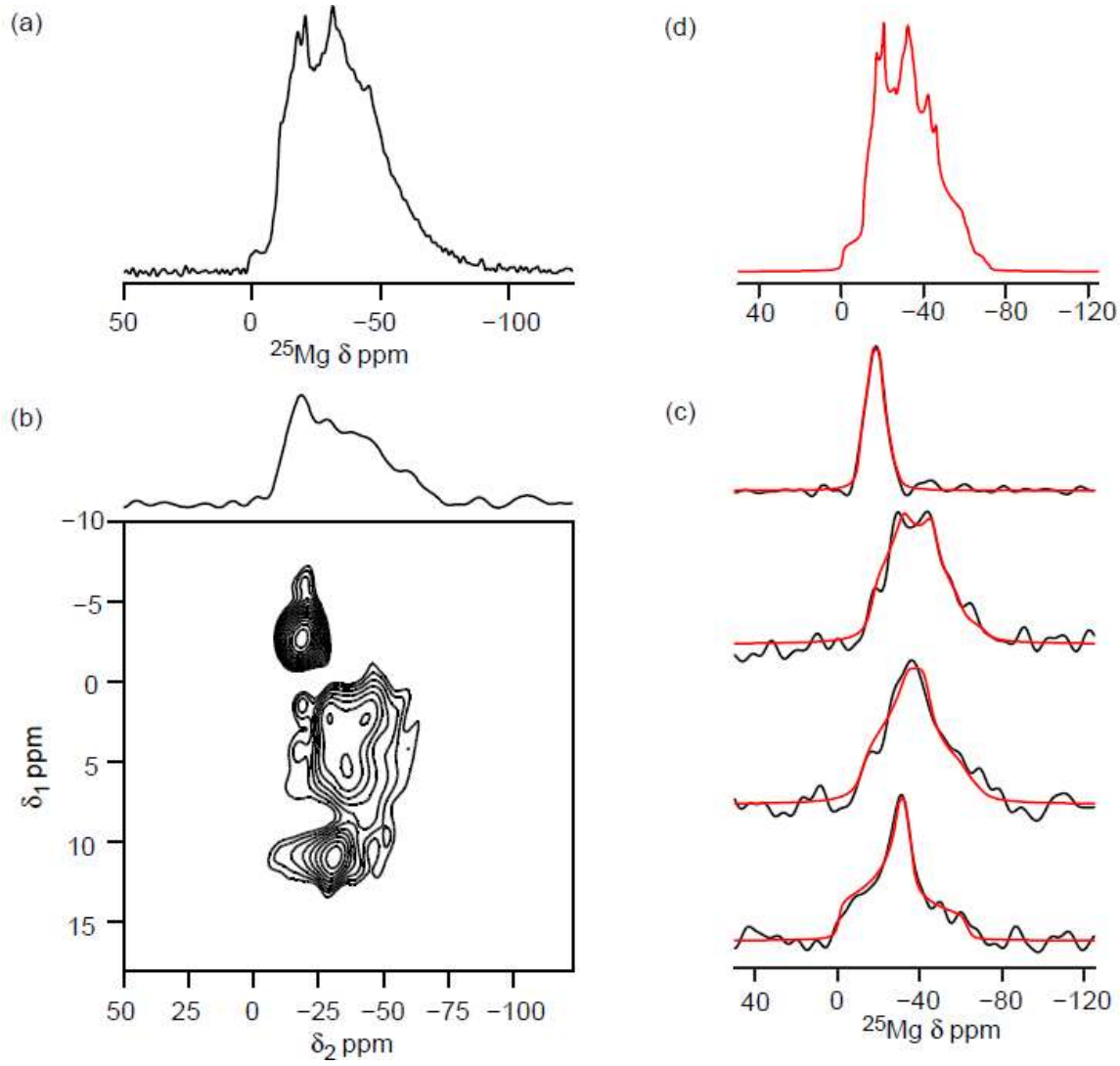
(a)
50
0
−50
−100
25Mg δ ppm
(b)
−10
−5
0
5
10
15
δ1 ppm
50
25
0
−25
−50
−75
−100
δ2 ppm
(d)
40
0
−40
−80
−120
(c)
40
0
−40
−80
−120
25Mg δ ppm

Table Caption

Table 1: Experimental[a] and calculated[b] ^{25}Mg NMR parameters (isotropic chemical shift, δ_{iso}, isotropic chemical shielding, σ_{iso}, quadrupolar coupling constant, C_Q, and quadrupolar asymmetry, η_Q)) for magnesium acetate samples.

Table

	δ_{iso} (ppm)	σ_{iso} (ppm)	C_Q / MHz [c]		η_Q	
	expt.	calc.	expt.	calc.	expt.	calc.
$Mg(OAc)_2 \cdot 4H_2O$						
Mg1	3 (0.4)	550.5	2.5 (0.01)	−4.8	0.74 (0.01)	0.76
$Mg(OAc)_2 \cdot H_2O$						
Mg1	−1.5 (6.5)	593.5	5.5 (0.3)	7.3	0.4 (0.2)	0.43
Mg2	−4.9 (5)	604.7	3.9 (0.3)	−4.9	0.6 (0.3)	0.63
α-$Mg(OAc)_2$						
Mg1	−0.9 (1.1)	607.1	5.0 (0.1)	−5.0	0.5 (0.2)	0.38
Mg2	−12.1 (10)	554.4	5.4 (0.5)	−5.5	0.8 (0.7)	0.79
Mg3	−18.5 (0.8)	597.9	1.4 (0.1)	−1.9	0.7 (0.3)	0.75
β-$Mg(OAc)_2$[d]						
Mg(a)	−0.5 (1)		3.2 (0.06)		0.92 (0.01)	
Mg(b)	−11.6 (0.5)	N/A	3.1 (0.09)	N/A	0.71 (0.05)	N/A
Mg(c)	−14.6 (1)	no crystal structure	3.2 (0.07)		0.48 (0.18)	
Mg(d)	−10.3 (0.5)		1.8 (0.03)		0.60 (0.1)	

[a] Experimental spectra were fitted using calculated data as a starting point.

[b] The calculated NMR values given in the table were obtained from structures where geometry optimisation was carried out with a fixed unit cell and where atomic coordinates were allowed to relax (FC). Calculated values for the other geometry optimised structures are given in Table 1 of the Supporting Information.

[c] The sign of C_Q is given for calculated values, but not determined experimentally.

[d] For β-$Mg(OAc)_2$ the sites are assigned letters as there is no crystal structure from which to assign specific numbered sites.

Graphical Abstract

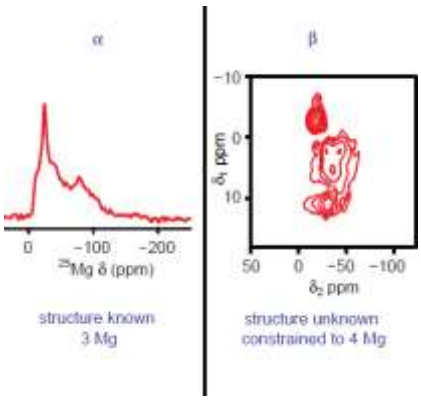

Structural Insight: ^{25}Mg Solid-State MAS NMR spectra for α- and β-$Mg(OAc)_2$ were obtained (see picture), providing NMR parameters for a MgO_7 site within a known structure, and providing structural insight for a phase with no known crystal structure.